



## Review

## X-ray structures of ferritins and related proteins

Robert R. Crichton\*, Jean-Paul Declercq

Department of Chemistry, Université Catholique de Louvain, Louvain-la-Neuve, Belgium

## ARTICLE INFO

## Article history:

Received 1 November 2009

Received in revised form 22 March 2010

Accepted 23 March 2010

Available online 2 April 2010

## Keywords:

Iron

Ferritin

Iron storage

Protein structure

X-ray structures

Bacterioferritin

Dps protein

Rubrerythrin

## ABSTRACT

Ferritins are members of a much larger superfamily of proteins, which are characterised by a structural motif consisting of a bundle of four parallel and anti-parallel  $\alpha$  helices. The ferritin superfamily itself is widely distributed across all three living kingdoms, in both aerobic and anaerobic organisms, and a considerable number of X-ray structures are available, some at extremely high resolution. We describe first of all the subunit structure of mammalian H and L chain ferritins and then discuss intersubunit interactions in the 24-subunit quaternary structure of these ferritins. Bacteria contain two types of ferritins, FTNs, which like mammalian ferritins do not contain haem, and the haem-containing BFRs. The characteristic carboxylate-bridged di-iron ferroxidase sites of H chain ferritins, FTNs and BFRs are compared, as are the potential entry sites for iron and the 'nucleation' site of L chain ferritins. Finally we discuss the three-dimensional structures of the 12-subunit bacterial Dps (DNA-binding protein from starved cells) proteins as well as their intersubunit di-iron ferroxidase site.

© 2010 Elsevier B.V. All rights reserved.

## 1. Introduction

Ferritins are the principal, if not the only, iron storage proteins in most living organisms throughout evolution – from man through invertebrates, plants and microorganisms [1]. They are tetracosameric protein shells (24-mers), made up of identical or similar subunits, which form a hollow protein shell. A non-toxic, water-soluble, yet bioavailable iron core is stored within this protein shell, often composed of ferric hydroxyphosphate micelles. The subunit structure consists of a closed, four-helical bundle with a left-handed twist with one crossover connection. The ferritin superfamily (see the chapter by Andrews [2] in this special issue of BBA for more details) includes ferritins and other ferritin-like proteins such as bacterioferritins (cytochromes  $b_1$ ) which bind haem between two subunits, as well as the dodecameric DPS proteins (ferritin homologues), which bind to and protect DNA and the N-terminal domain of peroxide-scavenging rubrerythrins, found in many microaerophilic and anaerobic bacteria and archae. They will all be discussed in this article. The ribonucleotide reductase-like family of proteins are also members of the ferritin superfamily, with a similar ferritin-like fold (for a review, see [3,4]). Like mammalian H chain ferritins and bacterial ferritins, they are characterised by carboxylate-bridged di-iron centres localised within the four-helix bundle, which seems to be a preferred biological scaffold for dioxygen binding and activation. Among the functions of this superfamily are radical generation in ribonucleotide reductases,

hydrocarbon desaturation in stearyl-acyl carrier protein  $\Delta^9$  desaturases and hydrocarbon oxidation in multicomponent monooxygenases, which catalyse hydroxylation of a variety of hydrocarbon substrates, including alkanes, alkenes and aromatics.

## 2. The apoferritin subunit

A representation of recombinant horse L apoferritin subunit as a ribbon diagram is presented in Fig. 1, showing the relationship of the secondary structure elements to the inner and outer surface of the 24-mer. Nearly three quarters of the 174 residues of the subunit are disposed within five  $\alpha$  helices designated A, B, C, D, E; corresponding approximately to residues 14–40, 49–76, 96–123, 127–161 and 163–173 (H chain numbering, see [1]). Helices A–D constitute a characteristic long central bundle of four parallel and anti-parallel helices, with the fifth short helix, E, butting on to one end of the  $\alpha$ -helical bundle. The four-helical bundle A–D shows a left-handed twist when viewed down the bundle axis.

There are short non-helical regions at the N- and C-termini and at the right-handed turns between the AB and the DE helices (this latter is particularly tight). Helices B and C are connected by the long loop BC (residues 78–94) which stretches along the length of the helical bundle. The N-terminus, the loop BC, and the helices A and C form the outside of the molecule (to the front in Fig. 1), whereas helices B and D face the inside surface. A break in hydrogen bonding at His 136 causes a kink in the long D helix, which allows it to extend to the external surface. This D helix kink occurs at a position where three subunits come together near the 3-fold axis, allowing a channel to form without disrupting the packing of the helices in the remainder of the

\* Corresponding author.

E-mail address: [Robert.crichton@uclouvain.be](mailto:Robert.crichton@uclouvain.be) (R.R. Crichton).

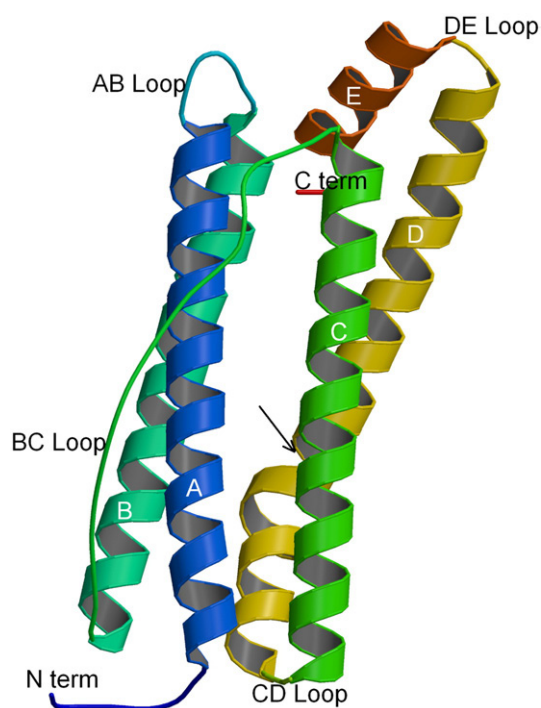


**Fig. 1.** Ribbon diagram of recombinant horse L apoferritin, PDB 2v2i, showing the relationship of the secondary structure elements to the inner and outer surface of the 24-mer. The outer surface (front) consists of helices A and C and the loop BC, while the inner surface (behind) is made up of helices B and D. Helix E is inclined at  $\sim 60^\circ$  to the four-helix bundle. The subunit is coloured progressively from blue at the N-terminus to red at the C-terminus. The kink in the D helix is indicated by the arrow. Produced with MOLSCRIPT [68].

four-helix bundle (see below). Within the subunit there are extensive side chain interactions. At the two ends of the helical bundle many side chains in the subunit interact to form tightly packed hydrophobic cores whereas in the centre there are a number of buried polar and hydrophilic residues which form a network of hydrogen bonds, and it is within this part of the subunit bundle that the most important changes between H and L subunits are situated.

The subunit is roughly cylindrical, a little more than 50 Å long and 25 Å wide. The N-terminus of the subunit lies on the outside surface of the assembled oligomer (Fig. 1) and makes a number of intra- and intersubunit interactions. The four long helices have intramolecular contacts which extend over a length of 35 Å, while the fourth helix, D, protrudes beyond this contact region. At the end of the D helix the chain folds sharply back on itself, placing the E helix at  $60^\circ$  to the principal helix bundle. Helices A, B and C are about 43 Å long, whereas the D helix is longer (52 Å) and the E helix is much shorter (16 Å).

Mammalian ferritins are typically heteropolymers made up of two subunits of distinct amino acid sequences, known as H (heavy, predominant in heart) and L (light, predominant in liver). For a 24 subunit molecule with two kinds of subunits, one can build 25 canonical<sup>1</sup> 'isoferritins' [5]. The H chains, as mentioned above, are characterised by a di-iron, ferroxidase centre, involved in the oxidation of  $\text{Fe}^{2+}$  to  $\text{Fe}^{3+}$ , whereas the L chains are thought to be involved in the nucleation of the iron core (see [1, 6]). The effective storage of iron in mammalian ferritins requires contributions from both types of subunits, which probably explains why we normally find heteropolymers rather than homopolymers. In contrast, plant and bacterial ferritins tend to be homopolymers with subunits which are more similar to mammalian H chains than to L chains, particularly in

that they possess the carboxylate-bridged di-iron centres (see below). Plant ferritins, which will not be considered here since no X-ray structures are available, contain both a typical H-type ferroxidase centre and all the amino acid residues characteristic of the nucleation centre of L-type subunits (see below) and could therefore be considered as H/L hybrids [7]. In prokaryotes we find two classes of ferritins, bacterial ferritins, designated FTNs, similar to mammalian H chain ferritins with a ferroxidase centre and a second class of ferritins namely the BFRs, bacterioferritins, which contain haem bound at the interface between two subunits as well as a ferroxidase centre.

Fig. 2 presents ribbon diagrams of the subunit structure of recombinant human H and horse L chain ferritins (HuHF and HoLF), non haem-containing bacterioferritin (FTN) from *Escherichia coli*, haem-containing bacterioferritin (BFR) from *Desulfovibrio desulfuricans*, and one of the DPS proteins from *Deinococcus radiodurans* [8–11]. What is immediately apparent is the striking similarity of the global subunit fold, particularly the central four helix bundle. Across the five structures presented in Fig. 2 superposition of the  $\text{C}^\alpha$  atoms of the four helices of the latter four ferritins with HUHF gives the following r.m.s. deviations: HuHF with HoLF, 0.44 Å for 117 atoms; HuHF with *E. coli* FTN, 1.73 Å for 117 atoms; HuHF with *D. desulfuricans* BFR, 1.69 Å for 117 atoms; HuHF with *D. radiodurans* DPS 1, 2.29 Å for 114 atoms. As would be expected, the loops linking the helices of the central bundle are much more variable. We first compare the two mammalian ferritins HuHF and HoLF and then compare the other three bacterial proteins with HuHF.

When we compare the two mammalian apoferritin subunits (Figs. 2a, b), superposition of the four helix bundle and the E helix shows an extremely high level of similarity (r.m.s. deviation of  $\text{C}^\alpha$  atoms 0.44 Å for 129 atoms) Likewise, the AB and CD loops as well as the long BC loop are remarkably similar. Only the DE turn is quite different; in HuHF it consists of three overlapping turns, whereas in HoLF it is a tight turn with only one residue between the end of helix D and the start of helix E (Fig. 3). Whereas in HuHF the BC loop and the DE turn appear to be the most mobile parts of the structure, in HoLF the BC loop does not appear to be more mobile than the rest of the subunit, while the much shorter DE turn appear to be either disordered or else highly mobile.

The *E. coli* FTN (Fig. 2c) is 17 residues shorter than HuHF. The N- and C-termini are shorter by 10 residues and 1 residue, respectively. The A–B and D–E turns each have two fewer residues and there are single-residue deletions in the BC loop and in the D helix. Superposition of the  $\text{C}^\alpha$  atoms of the four helices gives an r.m.s. deviation of 1.73 Å for 117 atoms. Over the whole main chain structure, the deviation is 1.93 Å for 150 atoms despite the low sequence identity (only 22%). The A helix is a little longer in FTN than in HuHF, as is the B helix, with the AB turn reduced from five residues to one residue. The BC loop follows a quite different trajectory, and the C helix is longer by one residue at the C-terminal end. In place of the kink in the D helix of HuHF due to deviations in  $\varphi$ ,  $\psi$  angles for residues 136 and 137, in EcFtnA where a residue is lost, there is a more gradual bend. The E helix is shorter in EcFtnA and is oriented almost at  $90^\circ$  to the main chain helix bundle. There are 37 residues which are identical between the two sequences; they are found clustered around the centre of the four-helix bundle. As we will see later, this central conserved region is associated with metal-binding sites and with the carboxylate-bridged di-iron ferroxidase centre referred to above.

The *D. desulfuricans* BFR structure (Fig. 2d) is much more similar to FTN than to HuHF. The A helix begins almost immediately without an N-terminal appendage, the B helix is one turn shorter, although the BC loop follows a very similar topography. Both the C and D helices are shorter, with a much tighter CD turn, and again, the orientation of the E helix to the helix bundle is close to  $90^\circ$ . While the detailed subunit structure differs significantly from HuHF, the conserved residues essentially again fall in the centre of the four helix bundle, as in FTN.

<sup>1</sup> Clearly, where the different subunits are within the tetrasomer, they can generate many times more geometrical isomers than this, more modest, biochemical estimation.

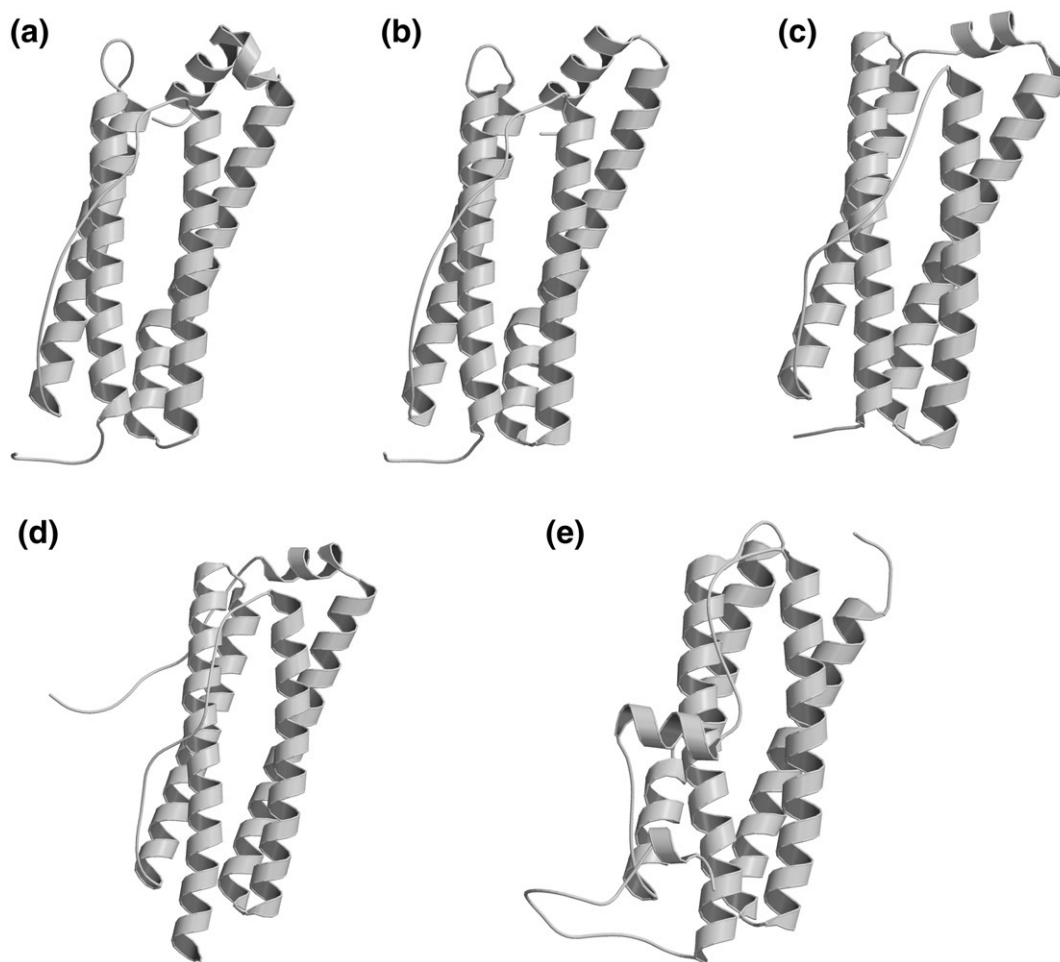


**Fig. 2.** Ribbon diagram of the subunit structure of mammalian H and L subunits, bacterioferritin (FTN) haem-containing bacterioferritin (BFR) and Dps protein. (a) human H chain ferritin, PDB 2fha; (b) horse L chain ferritin, PDB 2v2i; (c) *E. coli* bacterioferritin (FTN), PDB 2htn; (d) haem-containing *D. desulfuricans* bacterioferritin (BFR), PDB 1nfv; and (e) *D. radiodurans* DPS protein, PDB 2c2u. Produced with MOLSCRIPT [68].

Although the ferritins and DPS proteins self-assemble to form respectively octahedrally symmetric 24-mers and 12-mers with tetrahedral symmetry, nonetheless their subunits have similar four-helix bundle structures (Fig. 2e). They differ, however, in the presence of the fifth short additional helix. In ferritins this is located at the C-terminus and is positioned along the 4-fold symmetry axis, whereas in DPS proteins, the extra helix is located between the second and third helices in the monomer bundle and helps to define the 2-fold axis in the oligomer [12].

Within the subunit there are extensive side chain interactions. However, in both HuHF and HoLF and in the two bacterial ferritin structures represented in Fig. 2, the four-helical bundle does not have a uniformly hydrophobic interior. At the two ends of the helical bundle many side chains interact to form tightly packed hydrophobic cores (Fig. 4). However, there is a central hydrophilic region (Fig. 5), sandwiched between these two hydrophobic cores. In this region there are a number of buried polar and hydrophilic residues which form a network of hydrogen bonds, and it is within this part of the subunit bundle that the most important changes between H and L subunits are situated. Within the L subunit, a buried salt bridge is formed between Lys 62 and Glu 107 and 141<sup>2</sup>, which contributes significantly to the stability of the L subunit [13]; Glu 107 also interacts with Tyr 34 (Fig. 5). Of the seven residues found in the central hydrophilic region within the subunit bundle in HoLF, only

three are conserved in HuHF (Tyr 34, Glu 61 and Glu 107). Although the central intrasubunit salt bridge between Lys 62 and Glu 107 is gone, both Tyr 34 and Glu 107 are in virtually identical positions in both proteins, as are Gln 141 and Glu 141 in HuHF and HoLF, respectively. However, the site that is formed in the H subunit is capable of binding and rapidly oxidising two ferrous ions; this constitutes the carboxylate-bridged di-iron site referred to earlier and is discussed in greater detail later. The constellation of residues constituting the ‘ferroxidase’ centre are found in all animal H chains, most plant ferritins and non-haem containing bacterial ferritins. All but two of them are also found in haem-containing bacterioferritins.

The contacts between helix E and the subunit helical bundle are mediated through hydrophobic interactions and hydrogen bonds. In both H and L subunits helical residues in the central bundle must be disposed in such a way that one side of the helix is predominantly hydrophobic and the other hydrophilic. The hydrophobic helical sides face each other in the largely apolar interior of the subunit while the hydrophilic groups lie mainly on the outside of the bundle.

### 3. The subunit dimer

A second characteristic structural feature of both ferritins and Dps proteins is their propensity to form dimers (Fig. 6). Indeed, even if the overall pathway, or pathways, of oligomerisation remain unclear, there is general consensus that the subunit dimer is almost certainly the first intermediate to be formed [14,15]. However, before discussing the subunit dimer, we should introduce the different

<sup>2</sup> The numbering of amino acid residues is based on the human H subunit.

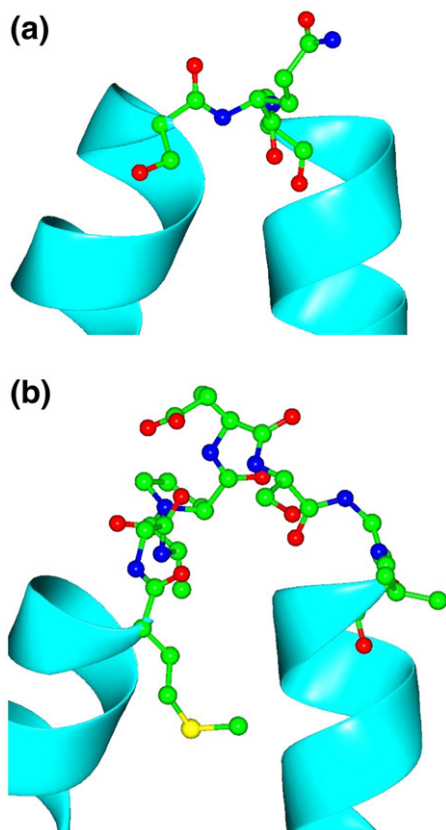


**Fig. 3.** Comparison of the DE turns in (a) HoLF (PDB 2v2i) and (b) HuHF (PDB 2fha). Produced with the programme CCP4mg [69].

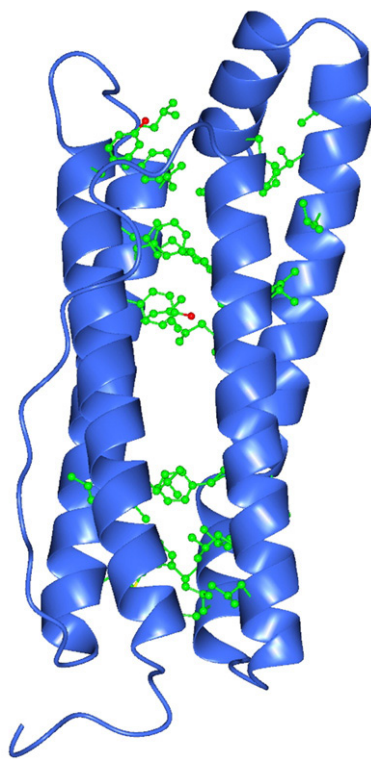


**Fig. 4.** Some of the hydrophobic interactions stabilising the hydrophobic cores at the two ends of the four helical bundle (illustrated by HoL, PDB 2v2i). Produced with the programme CCP4mg [69].

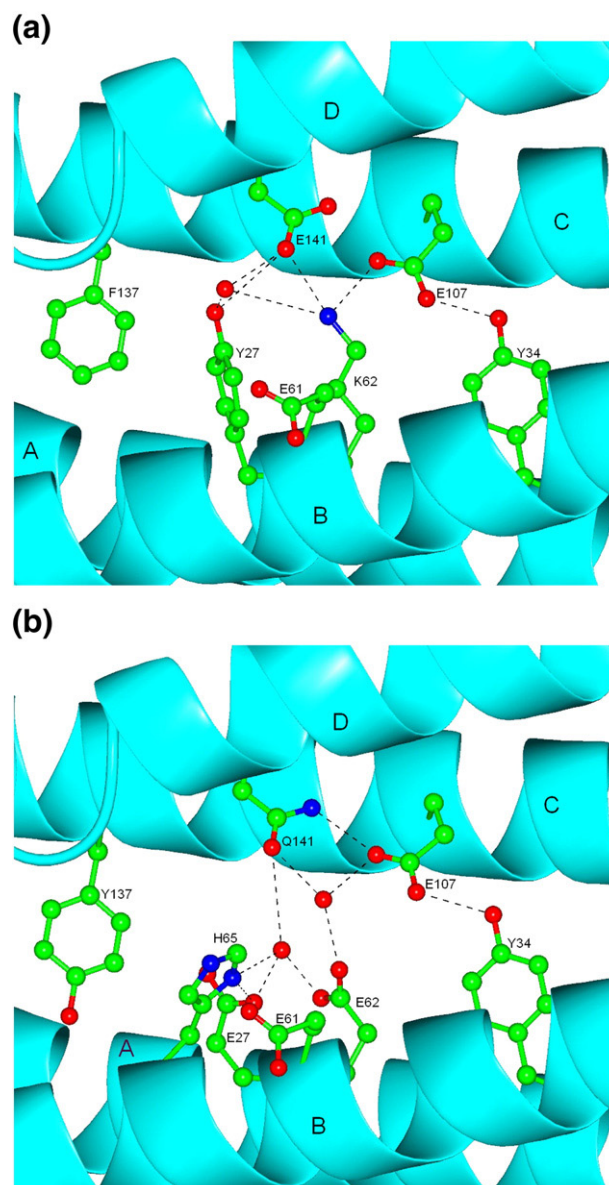


**Fig. 5.** The salt bridge in HoL in the central hydrophilic region of the four helical bundle, PDB 2v2i (a), compared to the same region of HuH, PDB 2fha (b). Produced with the programme CCP4mg [69].

interfaces between subunits in the global tetrasomer (24-mer). The packing of subunits within the shell and the intersubunit interfaces is shown schematically in Fig. 7a. Each subunit I interacts with six other subunits (II–VII). Fig. 8 gives a more detailed view of the subunit–subunit interactions at the interface for recombinant HoLF (the I–II interactions as indicated in Fig. 7). The two participating subunits are related to one another by a 2-fold rotation, such that the E helices are at opposite ends of the dimer. The interface involves the helices A and B, as well as the BC loops, the N-terminus and the AB turn. There is extensive contact between the two subunits along this long (22 Å) interface, which can be divided into two equivalent, symmetry-related halves involving many hydrophobic residues. There are several hydrophilic interactions clustered at the ends of the interface, including hydrogen bonds between the N-terminus of subunit I with the AB turn of II and between the ends of helix A(I) and helix B(II).

At the heart of the interface is an intersubunit four-helical bundle made up by helices A and B of one subunit (I) and helices A' and B' of the symmetry-related subunit (II). This bundle buries a number of hydrophobic residues from the solvent and in the process creates an

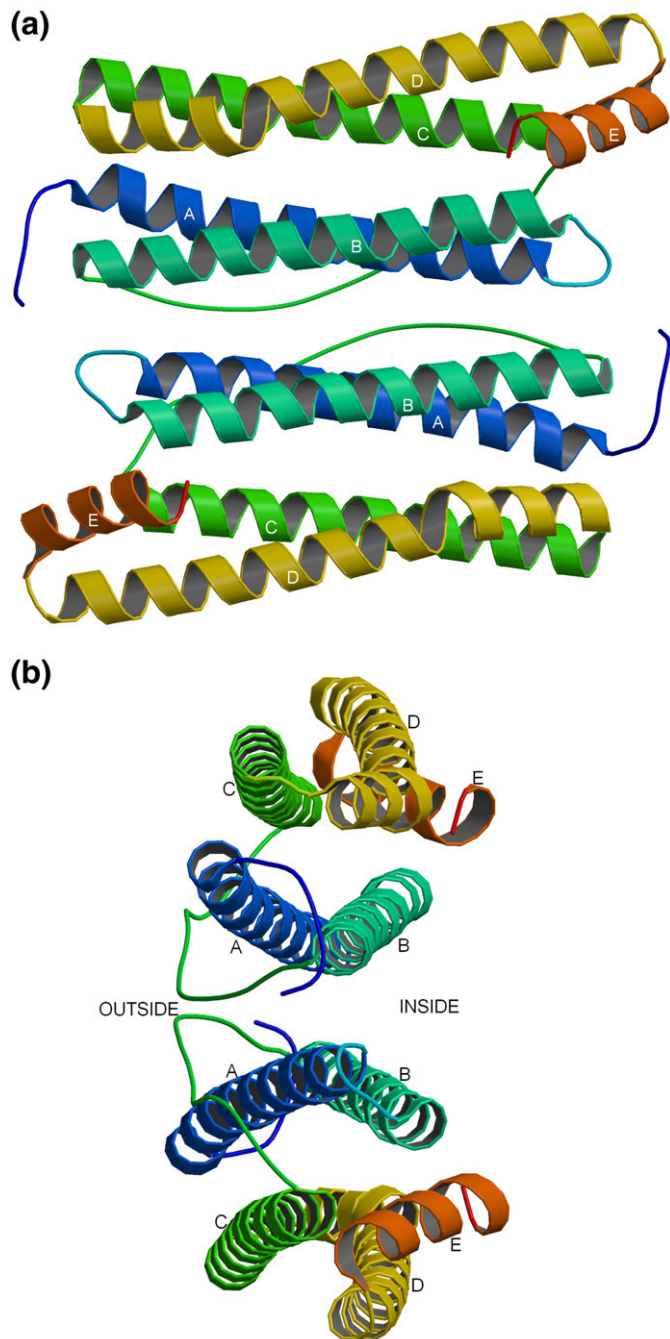


**Fig. 6.** Subunit homodimer of horse L chain apoferritin. (a) and (b) show orthogonal views of the homodimer of E53,56,57,60Q + R59M recombinant horse L chain apoferritin co-crystallized with haemin at pH 5.5 [Protein Data Bank (PDB) access code 2v2p], formed by two identical subunits. The subunits are coloured progressively from blue at the N-terminus to red at the C-terminus. Produced with MOLSCRIPT [68].

axis of 2-fold symmetry. The two BC loops form a section of antiparallel  $\beta$ -sheet within the dimer interface, and the interdigitation of hydrophobic side chains from BC and BC' between those from A and A' prevent contact between helix A and its dyad related A'. This also causes helices B and B' on the inside surface of the molecule to be held apart, resulting in the formation of a partial groove on the inside surface. In HuHF, Arg 63 stretches across this groove, forming an intrasubunit, intrahelix salt bridge with Glu 67. In contrast, in HoLF the two guanidino side chains of Arg 63 of BI and BII face each other across the groove and point into the cavity. In L chain apoferritins, towards the centre of the interface, a cluster of four glutamate side

chains from the B helix (Glu 57, 60, 61, 64) extend into the cavity in a diamond-shaped array and are thought to participate in iron micelle formation (see later). In contrast, in HuHF, His 60 lies within the interface rather than pointing into the cavity like Glu 60 in HoLF. As we will see later, it is in this relatively uncrowded central pocket in the interface that porphyrins are found to bind.

#### 4. The apoferritin protein shell

The compact, symmetrical and extremely stable apoferritin shell is the outcome of the assembly of 24 subunits, usually with octahedral

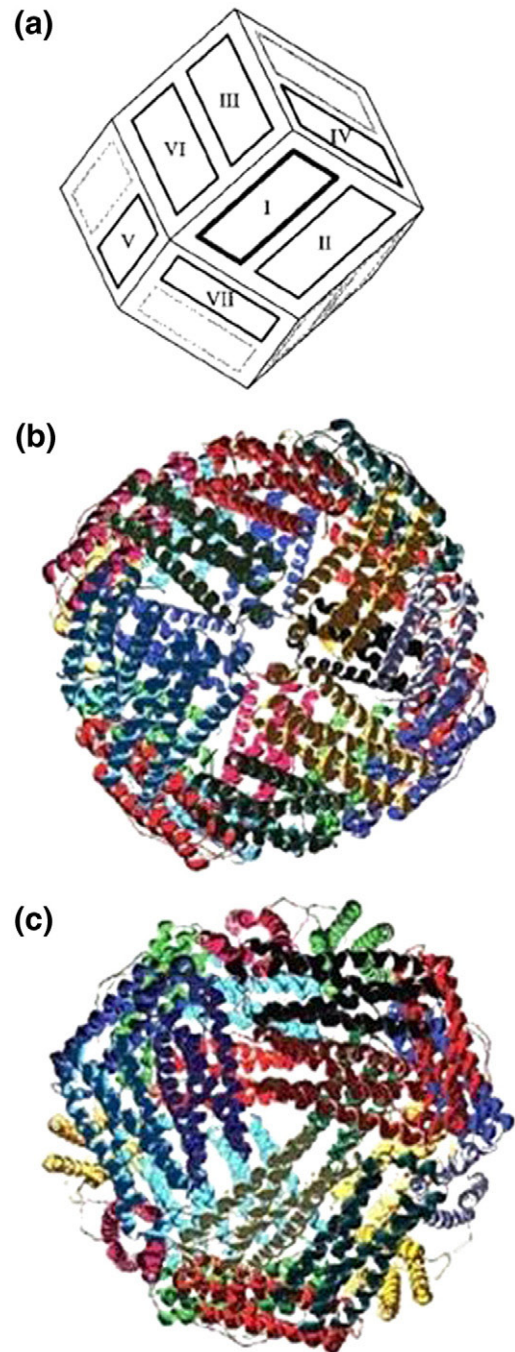


**Fig. 7.** Ferritin subunit symmetry relations. (a) Schematic diagram illustrating the relation between symmetry-related subunits. (b) View of the ferritin molecule down the 4-fold symmetry axis. (c) View of the ferritin molecule down the 3-fold symmetry axis (from [70] with permission from the Royal Society of Chemistry).

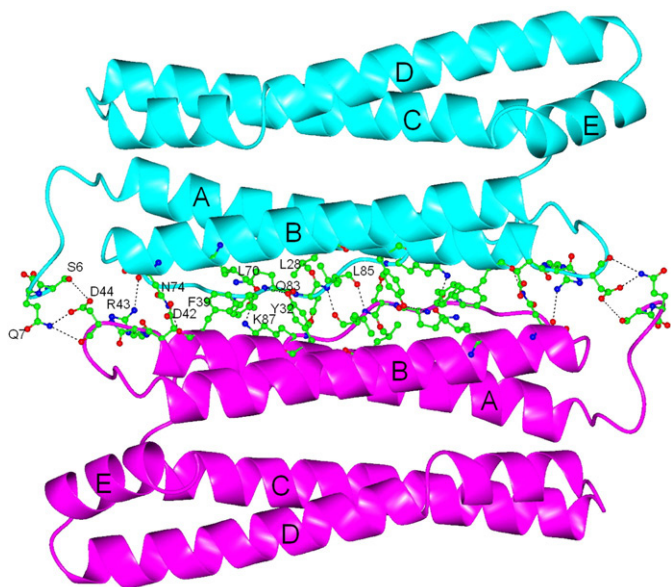


**Fig. 8.** Some of the hydrogen bonding interactions at the interface between subunits I and II of horse L chain ferritin (PDB 2v2i). Produced with the programme CCP4mg [69].

432 symmetry<sup>3</sup>. The shell has the approximate geometry of a rhombic dodecahedron, the faces of which consist of two subunits related by a 2-fold symmetry axis at its centre (e.g., I and II or III and VI). The subunit arrangements, viewed down the 4- and 3-fold axes of symmetry are presented respectively in Fig. 7b and c.

The other long side of subunit I interacts with the ends of subunits III and VI, while the two ends of subunit I also interact with subunits IV and VII (Figs. 7 and 9). Most of the intersubunit interactions involving both hydrophobic and hydrophilic interactions lie within these interfaces, between the 3-fold and 4-fold axes. The 3-fold axis related interactions I–III and IV–I are identical, as are those around the 4-fold axis (I–VI and VII–I), while there are only limited contacts across the 4-fold axis (I–V). In the second long interface (I–III and I–VI) the ends of subunits III and VI butt onto the other long side of subunit I contributed by helices C and D. Close to the 3-fold axis, there is an intersubunit salt bridge between Asp 139 (I) and His 128 (III) (replaced by a hydrogen bond between Asn 139 and His 128 in HuHF), which links the N-terminal end of helix D (III) to a position near the kink in helix D (I) (Fig. 9a). The N-terminus of subunit III make several interactions with the C and D helices of subunit I, and further along this interface there are interactions between apolar residues in neighbouring E helices of subunits I and VI (Fig. 9c) and hydrogen bonds between main chain oxygen atoms of the C-terminus of helix A and the AB turn of subunit VI to side chains at the end of helix D of subunit I (Fig. 9c). Fig. 9b presents the few contacts across the 4-fold axis between subunit I and subunit V, consistent with the reduced solvent accessibility. There are small channels at the axes penetrable by a 2 Å diameter probe [8].

There are two clearly discernable channels leading from the outside to the inside of the protein shell along the 4-fold and 3-fold axes of symmetry. A hydrophobic region is found on the surface of one face of the E helix, comprising Leu 165, Tyr 168, Leu 169, Leu 173 (His in H chains), together with Leu 158 near the C-terminus of helix D. In the oligomeric L chain protein structure this second hydrophobic patch is buried in the six channels along the 4-fold axes (Fig. 7b). This

is a left-handed bundle of four parallel E helices, which are lined by 12 leucine residues, Leu 165, Leu 169 and Leu 173 which lie along one edge of each of the E helices of four neighbouring subunits; this gives a long apolar channel, 12.5 Å in length, and relatively narrow – it is accessible to a 2 Å diameter probe [8]. The E helices protrude a short distance into the cavity. The narrowest part of the channel is near the outer surface of the protein shell, whereas in HuHF it is narrowest at the cavity end. Leu 173 at the cavity end of the channel in HoLF is replaced by His 173 in HuHF, while the other two Leu residues are conserved. The E helices of HoLF and other vertebrate ferritins lie roughly parallel with the 4-fold axis, making a short, left-handed, four-helix bundle. In contrast, in EcFtnA, the N-terminal ends of the E helices lie close together near the outer surface of the molecule but, towards their C-termini, the E helices point away from the symmetry axis such that the channel widens towards the inside of the molecule [18].

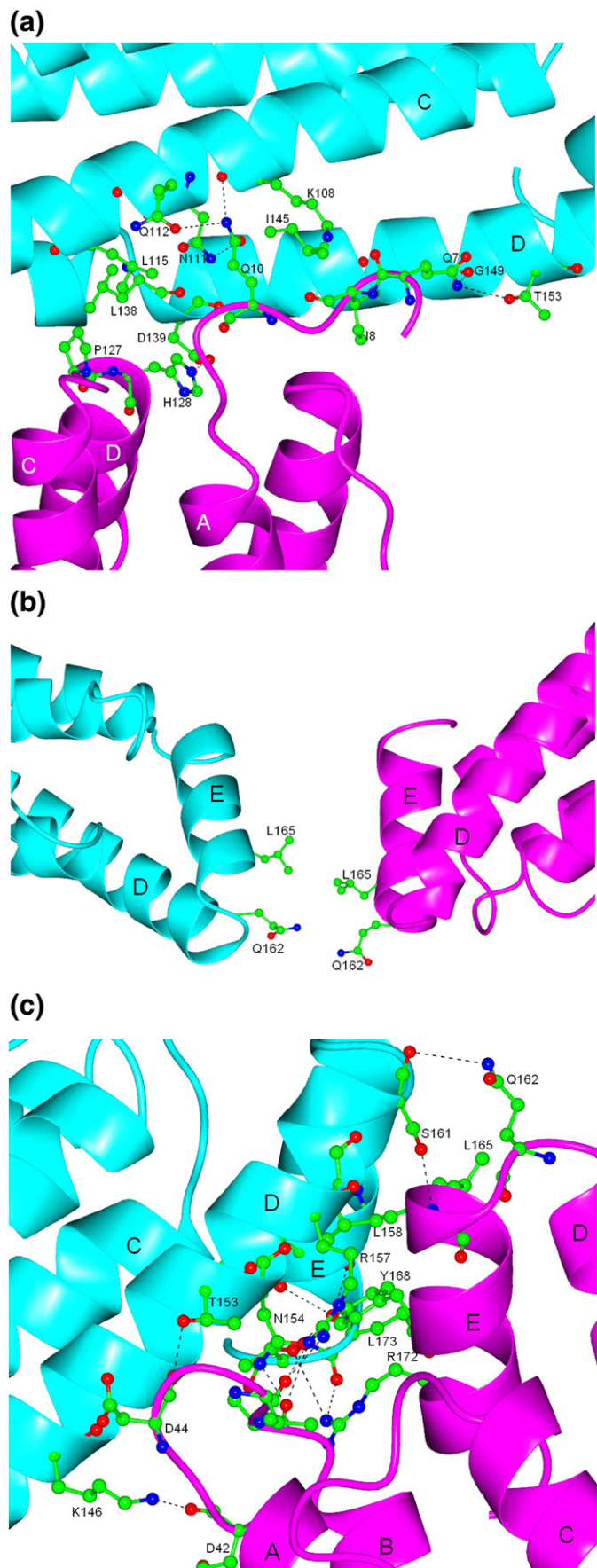
The eight 3-fold axes (Fig. 7c) are funnel shaped with a wider entrance at the outside of the molecule and a narrow passage (3.4 Å wide and about 6 Å long). The amino acid residues which neighbour and line these channels include residues from the C-terminus of helix C and those of the N-terminus of helix D. These residues (117–137) are highly conserved in both L and H subunits although there are a number of positions where H chains differ from L chains. Many of the H for L changes are found in or close to the wider end of the channel, whereas the narrow region is highly conserved in all ferritins. It is extremely hydrophilic in the narrow inner region, with three Glu 134 residues, towards the outer surface of the protein shell, and three Asp 131 residues, towards the inner surface (one from each of the three D helices), which are conserved in both H and L subunits, and predominantly hydrophilic in its wider entrance region. The funnel-shaped design of the channels could allow ions or molecules approaching the shell to find these channels more easily than if they were narrow throughout their length of about 12 Å. In the crystals the clusters of Glu and Asp residues each bind a Cd<sup>2+</sup> ion. In bacterial ferritins there are also 12 major channels (MC) through the protein shell occurring where one subunit dimer meets another [19].

## 5. A prettier shell

This is the subtitle of an article on the secreted insect ferritin from the cabbage looper *Trichoplusia ni* [17], a notorious North American parasite of brassica (cruciferous) plants, including, obviously cabbage! However, the most extraordinary characteristic of this eukaryotic ferritin is not only that it assembles its 24 subunit structure with tetrahedral (23) symmetry, as mentioned earlier, but that the tetracosameric shell is made up of an equal number of H and L chains arranged in dimers (Fig. 10).

Octahedral symmetry ferritin shells contain three 4-fold symmetry axes, four 3-fold axes and six 2-fold axes. The exact 4-fold axes in octahedrally symmetric ferritins become pseudo 4-fold in tetrahedrally symmetric ferritin, and there are two distinct local 3-fold axes, one made of three H chains and one made of three L chains. The 2-fold axes are lost because the 2-fold symmetric homodimers are replaced by heterodimers of H and L chains. Assembly of ferritin shells with octahedral symmetry is thought to begin with the formation of homodimers [8,14,15]. The molecular basis for the specificity of heterodimer versus homodimer assembly in *T. ni* ferritin appears to be associated with two Trp residues at the I/II interface in the respective subunits (Fig. 11). The L chain Trp 84 position is an Arg in mammalian ferritins and Met in bacterioferritin, both involved in binding of porphyrins [20, 21]. The corresponding residue on the *T. ni* H chain is Arg 68, which makes cation–pi interactions [22] with L chain residues Trp 84 and Tyr 53 and forms a salt-bridge with L chain Asp 81. This intersubunit salt-bridge in insect ferritins replaces an L chain intrasubunit salt-bridge in mammalian ferritins. The second tryptophan at the I/II interface of *T. ni* ferritin, H chain residue Trp 14

<sup>3</sup> Exceptions are the FTN from the hyperthermophilic Archeon *Archeoglobus fulgidus* the 24 subunits of which assemble into a shell with tetrahedral (23) symmetry [16] and the secreted insect ferritin from the cabbage looper/tiger moth *Trichoplusia ni* which has an equal number of H and L subunits, and also has tetrahedral (23) symmetry [17] (of which more later).



together with H chain Ile 10 and Ile 15 forms a hydrophobic binding pocket for L chain Tyr 65. Computer models of insect H/H and L/L homodimers reveal that the described interactions around both tryptophan residues are only possible in the heterodimeric H/L structure.

## 6. Bacterial ferritins

In bacteria we find two types of ferritin, the archetypal ferritins of the H type which are also found in eukaryotes (usually designated FTN) and the haem-containing bacterioferritins (designated BFRs). Most FTNs, including that from the hyperthermophilic Archaeon *Pyrococcus furiosus* [23] have the canonical octahedral (432) symmetry of archetypal ferritins. In contrast, the ferritin from the hyperthermophilic Archaeon *Archaeoglobus fulgidus* has a novel quaternary structure, its 24 subunits assembling into a shell having tetrahedral (23) symmetry [16], despite having only one type of subunit. The difference in assembly opens four large (~45 Å) pores in the *A. fulgidus* ferritin shell (Fig. 12).

The BFRs were first unequivocally identified by Steifel and Watt [24]. Since then they have been isolated from many bacteria and identified in the gene sequences of quite a few others. They are made up of 24 H chain-type subunits and in most cases are homopolymers, although some, like the BFRs of *Pseudomonas aeruginosa*, *P. putida* and the cyanobacterium *Synechocystis* contain two subunit types [25–27]. They all contain an iron-protoporphyrin as an integral part of the protein, usually Fe(II)–protoporphyrin IX (haem), although in *Desulphovibrio desulfuricans* BFR the haem cofactor is Fe-coproporphyrin III [28]. The *E. coli* BFR subunit has hydrophobic regions at each extremity of its four helical bundle with at the centre a hydrophilic region, which contains five of the residues of the ferroxidase site which is described below. The mostly hydrophobic long I–II intersubunit contact supplies a nesting site for haem (Fig. 13), with two symmetry-related Met residues as axial ligands to the metal centre. The 3-fold channels are hydrophilic in most BFRs as are the 4-fold channels – unlike the hydrophobic character of the latter in mammalian ferritins.

## 7. Access to the interior of the protein shell

Since the role of ferritins is to store a water-insoluble ferric iron core inside the water-soluble protein shell, it is logical to assume that all substances involved in ferritin iron deposition or mobilisation –  $\text{Fe}^{2+}$ ,  $\text{Fe}^{3+}$ ,  $\text{O}_2$ , reductants and chelators – need to gain access to the interior of the apoferritin protein shell. This topic is discussed in greater detail in the chapter by Watt [29] in this special issue of BBA. The most likely route for iron entry into mammalian ferritins is via the 12 Å long hydrophilic 3-fold channels [30–37]. Electrostatic potential energy calculations on these channels in mammalian H and L chain ferritins [19, 38, 39] support this view. The negative outer entrance is surrounded by patches of positive potential, and this arrangement leads to electrostatic fields directing cations towards the channel entrance, the 3-fold route. The region of negative potential extends through the 3-fold channel to the interior of the molecule, such that  $\text{Fe}^{2+}$  translocation through the channel would be driven by an electrostatic gradient. The role of the 3-fold channel in the entry of divalent cations into the interior of the protein is further documented by a number of crystallographic studies on human, horse and mouse ferritins in which divalent metal ions ( $\text{Zn}^{2+}$  and  $\text{Cd}^{2+}$ ) are found bound specifically in these channels [8, 40–42]. Indeed, using  $\text{Zn}(\text{II})$  as a

**Fig. 9.** Some of the hydrogen bonding interactions at the interface of horse L chain ferritin (PDB 2v2i): (a) between subunit I and III (same as IV–I); (b) between subunit I and V; (c) between subunit I and VI (same as VII–I). I, cyan; III, V and VI, magenta. Produced with the programme CCP4mg [69].

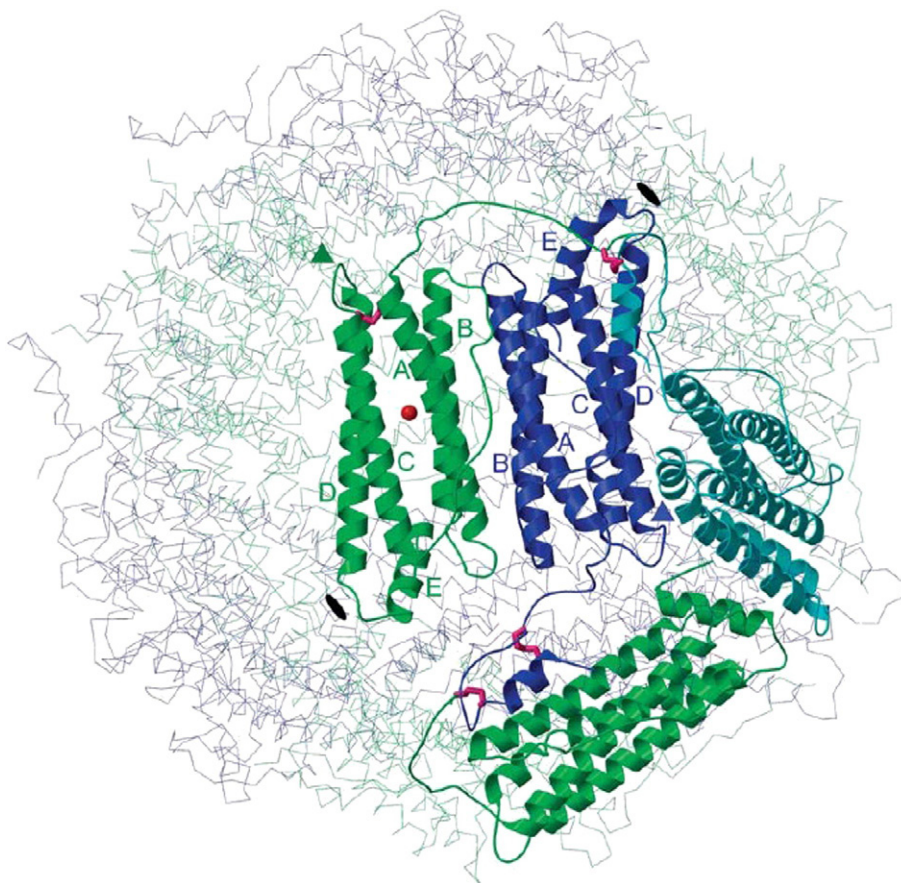


**Fig. 10.** Structures of *T. ni* ferritin H and L chains. Ribbon diagrams of the H (green) and L (blue and light blue) subunits. The  $\text{Fe}^{3+}$  at the ferroxidase site is shown in red. Also shown are the approximate locations of the 3-fold axes (blue and green triangles) and the pseudo 4-fold axes (black ovals). Disulfide-bonded cysteine residues are shown in magenta in ball-and-stick representation. The N-terminal region of each subunit extends on the outside of the ferritin shell and forms a disulfide bond with a non-adjacent subunit of the opposite type. Helices A–E are labeled in green for the H chain and in blue for the L chain (from [17], with permission from Elsevier).

redox-stable alternative for  $\text{Fe(II)}$ , Fig. 14 illustrates the way in which  $\text{Zn}^{2+}$  ions can transit through this channel, using the configurational flexibility of a key cysteine residue (Cys 130), in a

manner reminiscent of the transit of  $\text{K}^{+}$  ions through the potassium channel [43].

Iron incorporation into the dodecameric ferritin-like Dps proteins (see below) also conforms to this general picture of an electrostatic

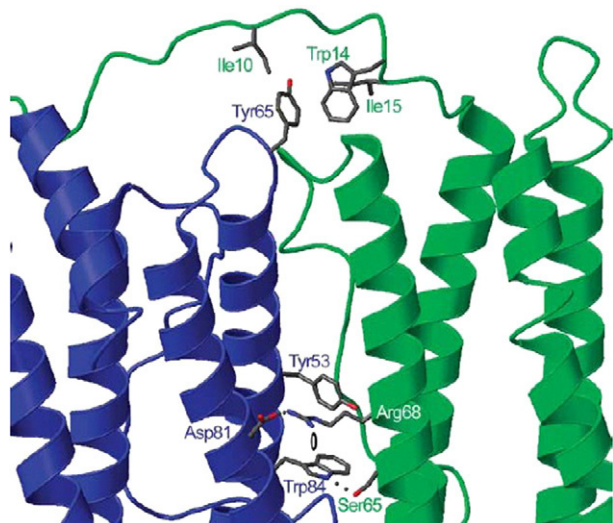


**Fig. 11.** Packing of the major H/L interface. Residues involved in key intersubunit interactions are shown in ball-and-stick representation. The H and L chains are coloured green and blue, respectively. Hydrogen bonds and salt-bridges are shown as broken lines. The location of the pseudo 2-fold axis is shown as an open oval (from [17], with permission from Elsevier).

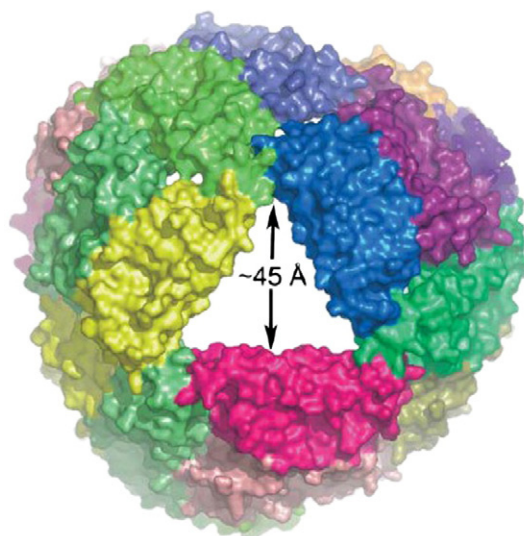


**Fig. 12.** Surface representation of the novel tetraicosameric assembly seen in the hyperthermophilic archaeon *A. fulgidus* ferritin. The molecule is viewed down one of four large pores at a 3-fold noncrystallographic symmetry axis (from [16], with permission from Elsevier).

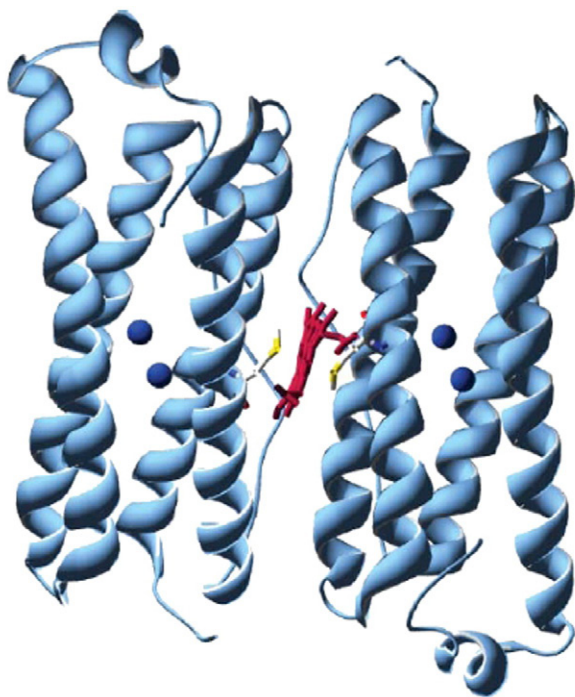


**Fig. 13.** The subunit dimer of *E. coli* BFR. The subunit dimer of *E. coli* BFR showing the intersubunit haem-binding site. The haem group (in red) is ligated by Met 52 and Met 52 (shown in grey/yellow) from the two subunits, respectively. The position of the intrasubunit ferroxidase centres of each subunit is shown (blue spheres) (from [70], with permission from the Royal Society of Chemistry).

gradient through the negatively charged hydrophilic pores at the 3-fold axes guiding iron to the ferroxidase centre [44, 45].

This situation contrasts to what is observed in bacterial ferritins, where no negatively charged 3-fold channel is observed when electrostatic potential surfaces are compared [19]. In contrast, clusters of negative charges appear in the bacterial proteins around the major channels referred to earlier, which extend to the interior of the

protein shell and that lead directly to the ferroxidase di-iron site. The iron atoms are located  $\sim 6$  Å below the channel entrance, which is approximately circular in shape with a radius of  $\sim 1.4$  Å. In bacterial ferritins, these channels may represent a possible alternative route for iron uptake through the protein shell, as opposed to access through the 3- or 4-fold axis channels.

## 8. The ferroxidase centre

Iron deposition in ferritins to form its mineral core is described in greater detail in the chapters by Bou-Abdallah [6] and Le Brun et al. [46] in this special issue of BBA. On the basis of kinetic considerations, the first step in the incorporation of iron into apoferritin was originally proposed to involve binding of ferrous iron to a di-iron centre, followed by the formation of a peroxo-diferric intermediate [47]. As the first X-ray structures of ferritins began to appear, it became clear that ferritins were members of the larger family of di-iron-carboxylate proteins [3]. In mammalian H chain ferritins, microbial ferritins (FTNs) and bacterioferritins (BFRs), the di-iron ferroxidase centre is located in the central region of the four-helix subunit bundle. The environment of representative ferroxidase centres of the Zn derivative crystal structure of recombinant human H chain ferritin, HuHFt [42], of *E. coli* ferritin, FtnA [18] and of *D. desulfuricans* bacterioferritin, Bfr [10], both in the presence of Fe, are shown in Fig. 15. They have many similarities – all three have a glutamate bridging both metal centres and each iron atom has an axial glutamate ligand. There are, however, many differences. FTNs from *E. coli*, *A. fulgidus* and *P. furiosus* have a third iron site, located some 6–7 Å away from sites A and B [18,16,23], while BFRs have a second bridging Glu [10,48].

## 9. Ferrihydrite nucleation site

The initial stages of iron incorporation into heteropolymeric mammalian ferritins require the ferroxidase sites of the protein; thereafter a nucleation site on the inner surface of the protein shell supplies ligands that can partially coordinate iron, while leaving some coordination spheres available for mineral phase anions. This then

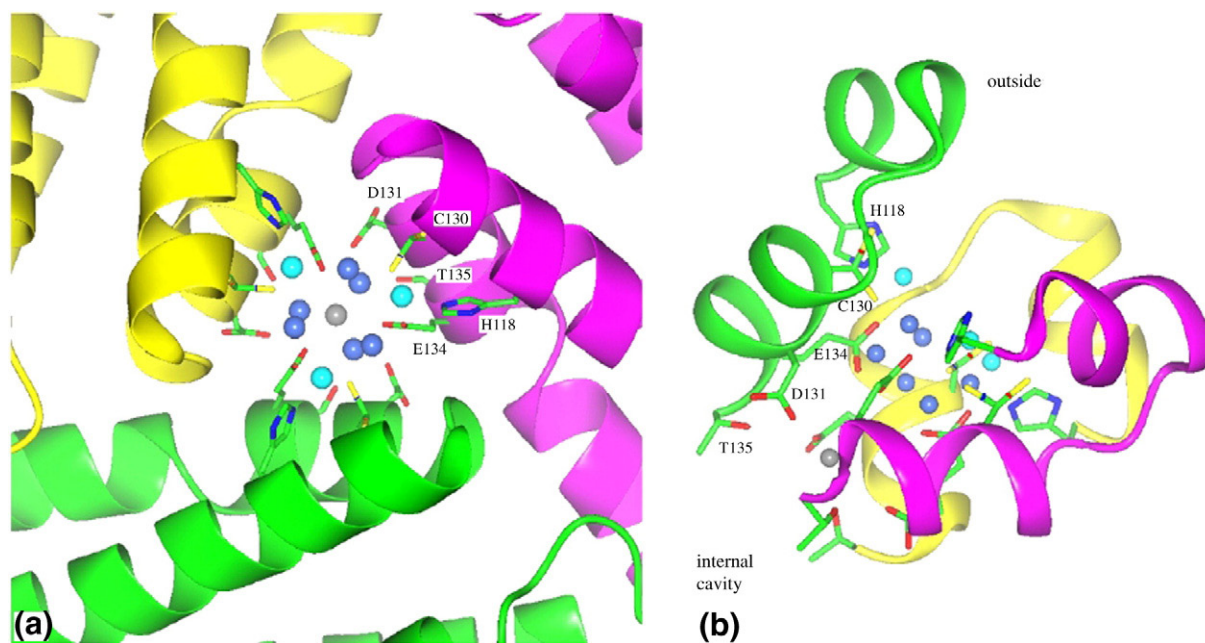


**Fig. 14.** The channel aligned on the 3-fold symmetry axis of recombinant human H chain ferritin shows binding to three zinc atoms and their symmetrically related subunits; the first is in the entrance of the funnel-shaped channel (in cyan), the second is in an alternative position (in blue) and the third is aligned on the 3-fold axis (in grey). The stoichiometry yields seven zinc cations per channel, i.e., 56 zinc cations per molecule. The two representations are (a) aligned on the 3-fold axis and (b) perpendicular to the axis (from [42], with permission from Elsevier).

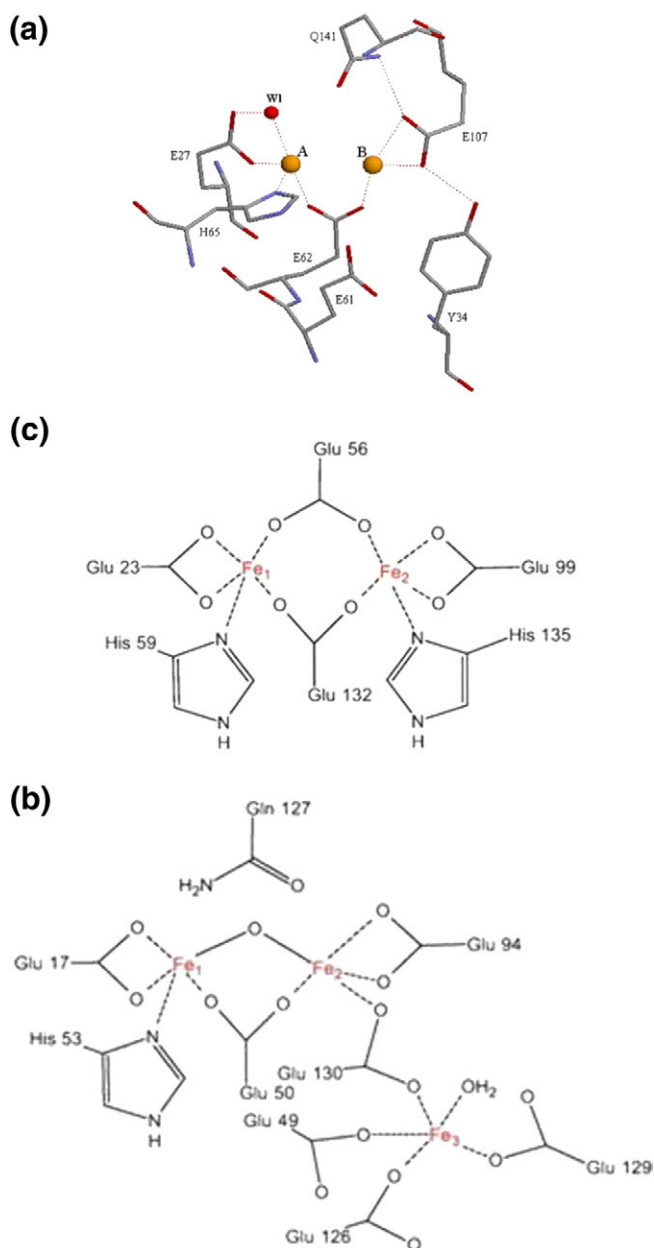


**Fig. 15.** Ferroxidase centre environment (a) from the Zn derivative of recombinant human H chain ferritin (from [42], with permission from Elsevier), (b) from *E. coli* ferritin, FtnA (from [18], with permission from Elsevier) and (c) from *D. desulfuricans* bacterioferritin (from [28], with permission from Elsevier), both in the presence of Fe.

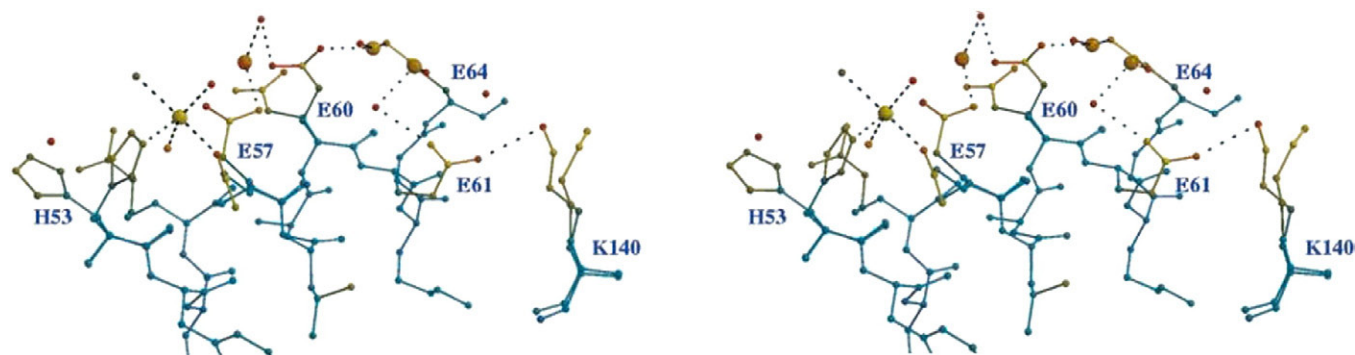


**Fig. 16.** Stereo view of the ferrihydrite nucleation centre of mouse L chain ferritin, with colours (from blue to red) as a function of atomic temperature factors (from 5 to 30 °Å<sup>2</sup>). From [54] with kind permission from Springer Science and Media.

allows the biomineralization process to proceed, with formation of one or more polynuclear ferrihydrite crystallites. The nucleation centres are made up of the highly conserved diamond cluster of glutamic acid residues Glu 57, Glu 60, Glu 61 and Glu 64, situated on the inner surface of the B helix at the subunit dimer interface of the L chain subunits [49–53]. A stereo view of the ferrihydrite nucleation site in the 1.2 Å resolution structure of mouse L chain ferritin determined under cryogenic conditions [54] is presented in Fig. 16. The orientation of the Glu 57, Glu 60, Glu 61 and Glu 64 side chains (which were highly disordered in previous structures determined at room temperature) is clearly revealed and allows a good description of the site taking into account the binding geometry of four Cd<sup>2+</sup> ions (used as a crystallization agent). The side chains of several residues (His 53, Glu 57 and Glu 60) adopt alternative conformations, directly associated with the four low-occupancy cadmium binding sites. In addition, the side chain of Lys 140, lying in the vicinity of the ferrihydrite nucleation site, also exhibits two alternative conformations, in one of which it interacts electrostatically with E61. This supports the conclusion of Santambrogio et al. [55] that this residue, which replaces a Glu in human and horse L chains, is responsible for the low level of iron incorporation by mouse L chain ferritin compared to human L chain ferritin.

## 10. DPS and other ferritin-like proteins

There are oligomeric proteins, like yeast frataxin [56], which are capable under particular *in vitro* conditions, of laying down an iron core and so, might be considered to be ferritins. However, frataxin does not have the structural characteristics of ferritins (frataxin is a compact  $\alpha\beta$  sandwich). Ferritin-like proteins can be defined as having the ‘ferritin fold’, and it is only with such proteins that we will concern ourselves here. The first to be described was the ‘ferritin’ from the Gram-positive bacterium *Listeria innocua* which sequesters 50–100 atoms of iron inside a protein cavity [57]. The primary structure showed a high similarity to the DNA-binding proteins designated Dps (DNA-binding proteins from starved cells), which are expressed in bacteria under conditions of oxidative or nutritional stress. Subsequent studies clearly established that the so-called *L. innocua* ferritin is indeed a Dps protein [58, 59]. As we saw earlier, the Dps monomer consists of a four-helix bundle, which closely resembles that of other ferritins (Fig. 2e) with greatest similarity to L chain ferritin (rmsd between C $\alpha$  positions 1.56 Å). There is a short helix in the middle of the BC loop in one subunit which interacts with the corresponding loop of a second subunit related by a 2-fold symmetry axis in the dimer (see below), while at the C-terminus the Dps protein lacks the fifth E helix. In some members of the Dps family, additional extensions are found at the N- or C-terminus, which are thought to be involved in interactions with DNA.

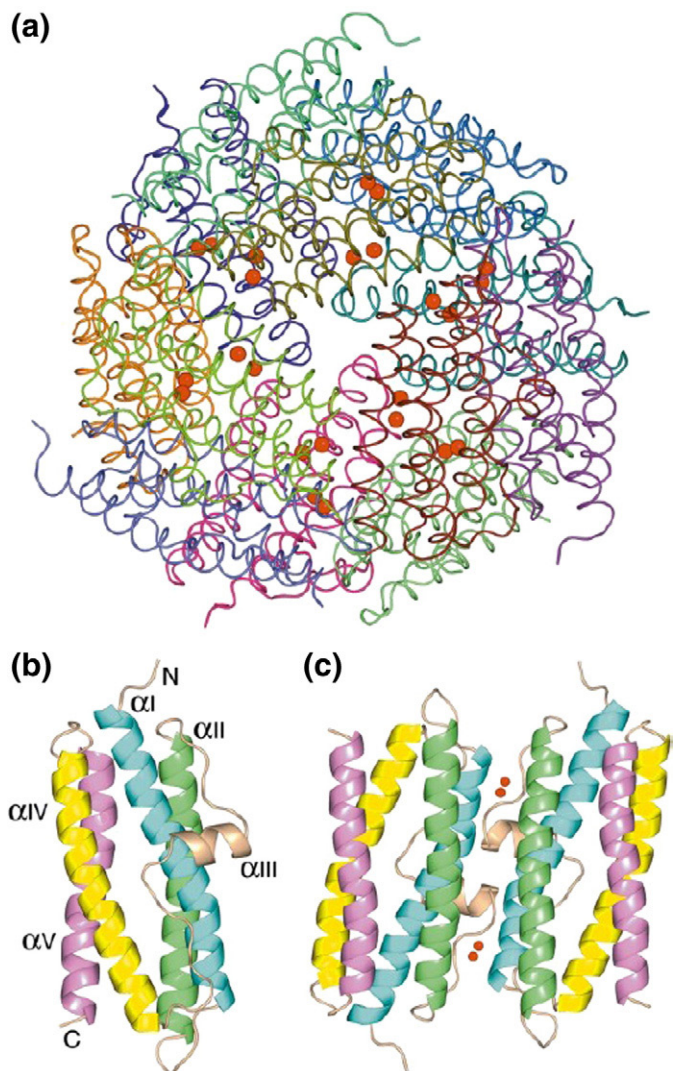


**Fig. 17.** The structure of *Bacillus brevis* Dps dodecamer (from [62], with permission from Elsevier). (a) The *BbDps* dodecamer. The 12 subunits are shown by the ribbon representation of their  $C^\alpha$  traces. The 24 iron ions at the ferroxidase centres inside the protein shell are shown as red spheres. (b) Ribbon diagram of the *BbDps* monomer. Helices  $\alpha I$ – $\alpha V$  are shown in different colours. (c) A *BbDps* dimer. The iron ions in the two ferroxidase centres at the dimer interface are shown as red spheres. The helices are coloured as in (b). The figures, except Fig. 17(b), were prepared with the program PyMOL (DeLano Scientific, San Carlos, USA).

However, in contrast to ferritins, Dps proteins are dodecamers with 23 symmetry (Fig. 17a). While the monomers (subunits) of DPS and ferritins share extensive homologies in their sequences and have very similar tertiary structures, they differ by the presence of a short, additional helix. In the ferritins, this fifth E helix is situated at the C-terminus and forms the channels which are located along the 4-fold symmetry axis. In contrast, the extra helix in DPS proteins is located between the B and C helices in the four helix subunit bundle, where it participates in defining the 2-fold symmetry axis. The consequence is that DPS proteins, self-assemble into a 23 symmetric tetrahedral dodecamer, whereas the ferritins, in general, self-assemble into a 24-mer with 432 octahedral symmetry. Even in the tetrahedrally (23) symmetric *T. ni* insect ferritin, the exact 4-fold axis becomes a pseudo 4-fold axis.

Each Dps subunit is a four-helix bundle structure, in which helices  $\alpha I$  and  $\alpha II$  are connected with  $\alpha IV$  and  $\alpha V$  through a short helix  $\alpha III$  in the middle of a long loop (Fig. 17b). In the *BbDps* crystal, a local 2-fold axis relates two subunits to form a dimer (Fig. 17c), which seems to be the assembly intermediate between monomer and dodecamer. The

two subunits are arranged side by side with the long axes of their helical bundles anti-parallel to each other. As a result, helix  $\alpha III$  in one subunit interacts with its counterpart in the other subunit. The other interactions at the dimer interface involve residues in helices  $\alpha I$ ,  $\alpha II$  and in the loop regions around  $\alpha III$  of each subunit. The spherical dodecamer (Fig. 17a) has a central cavity of  $\sim 40$  Å diameter in which an iron core of up to  $\sim 500$  Fe (III) atoms can be deposited [58, 60]. This corresponds to an internal cavity about one eighth that of typical ferritin shells, in excellent agreement with the respective capacity to store iron (500 versus 4500 atoms per oligomer). The relatively large negatively charged channels along the 3-fold axes may provide the pathway for iron entry into the negatively charged internal cavity (Fig. 17a).

Initial crystallographic studies on the Dps protein of *E. coli* led to the claim that Dps proteins did not have a ferroxidase centre [61]. The structure of *L. innocua* 'ferritin' revealed a single iron-binding site at the dimer interface, and on the basis of that structure and the ferritin-

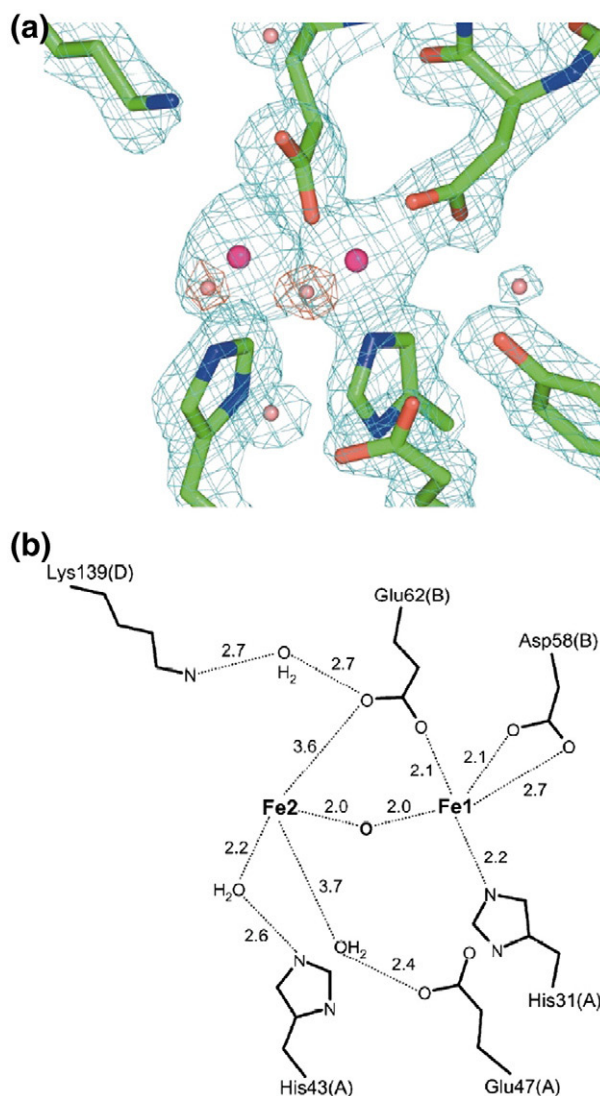


**Fig. 18.** The di-nuclear ferroxidase centre *Bacillus brevis* Dps dodecamer (from [62], with permission from Elsevier). (a) Electron densities at one of the di-nuclear ferroxidase centres at the dimer interface. The  $(2F_o - F_c)$  map is coloured in light blue and contoured at the  $1.4\sigma$  level. The two iron ions have the highest density values in the map, which are  $12.7\sigma$  and  $7.2\sigma$ . The existence of two water molecules at the di-iron site is revealed by the superimposed  $(F_o - F_c)$  map, which is coloured in red and contoured at the  $4.0\sigma$  level. The iron ions and water molecules are shown as spheres, coloured in magenta and light orange, respectively. (b) A drawing of the coordination of the iron ions at the di-nuclear centre. The coordination is indicated by dotted lines and distances (in Å).

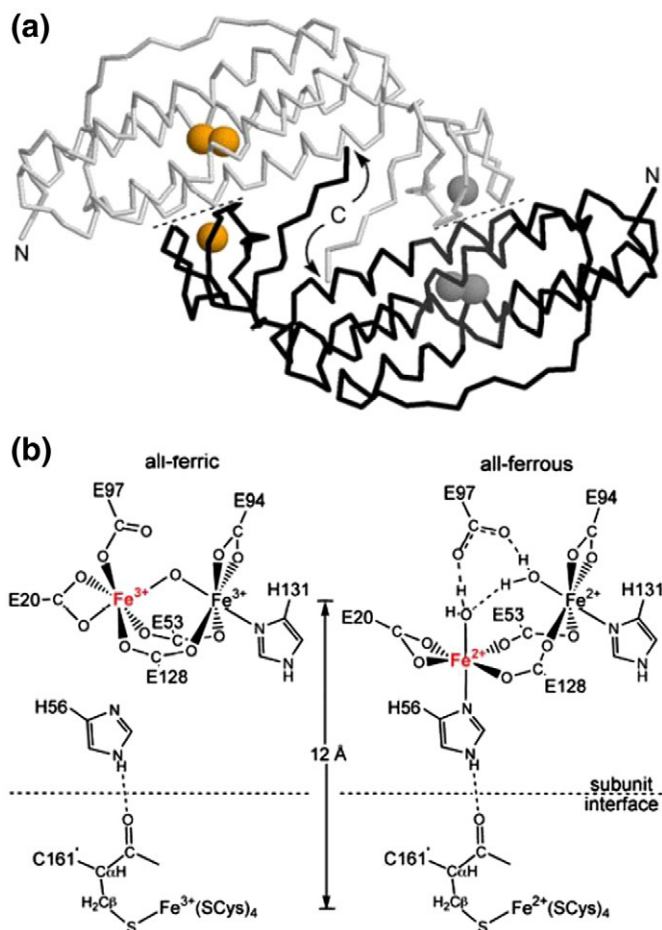


**Fig. 19.** Overall topology and redox-induced iron movement in *D. vulgaris* rubrerythrin (DvRbr). (a) Structure of the head-to-tail DvRbr homodimer backbone viewed along the 2-fold rotation axis with individual subunits indicated by light grey and black. N-termini and C-termini are indicated. Spheres represent iron atom positions (the rubredoxin-like domain is situated at the C-terminus, while the di-iron oxo site is in the middle of the four-helix bundle); orange spheres indicate the active site oriented approximately as in (b). Dashed lines indicate subunit interfaces. (b) Schematic structures of the iron sites in the all-ferric (left) and all-ferrous (right) DvRbrs. Fe1 (moving iron) is highlighted in red (from [66], with permission from Springer).

like activity of the *L. innocua* protein, it was postulated that a di-iron ferroxidase centre must exist, although efforts to reveal its existence failed [60]. However, the structure shown in Fig. 18 for the Dps of *Bacillus brevis* confirmed that a di-iron ferroxidase centre certainly does exist [62]. However the coordination is looser at one of the two sites – the single iron site in *L. innocua* Dps corresponds to site 1 in Fig. 18. The ferroxidase centre possesses unique features among all the di-iron proteins identified so far. Dps does not have a similar single di-iron site within the four-helix bundle of the subunit. Instead, two neighbouring dinuclear iron-binding sites are present at the dimer interface inside the dodecamer (Fig. 17c), related by the local 2-fold axis. They are located in a shallow groove formed by helices  $\alpha$ I and  $\alpha$ II from one subunit and their symmetry-related counterparts from the other subunit. One might consider that these helices at the dimer interface form a special four-helix bundle, which accommodates not one but two di-iron sites. The ligands to the pentahedral Fe 1 (Fig. 18) come from two subunits, while the more loosely coordinated Fe 2 has only one direct protein ligand, the bridging carboxylate Glu 62 (B) with additional water mediated contacts to Glu 47 (A) and His 43 (A).

It has been suggested [57, 61] that Dps and *L. innocua* Dps proteins represent examples of a family of ancestral dodecameric protein which had as function to trap, but not to mineralize, metal ions, and that the ability to efficiently oxidise and mineralize iron and to form 4-

fold interactions came later. The hollow-cored dodecameric motif exemplified by Dps has clearly been adapted to a number of functions, since in addition to DNA-binding and iron storage, other family members include a novel pilin, a bromoperoxidase and several other proteins of unknown function [61].

Rubrerythrin is a homodimeric non-haem iron protein found in many air-sensitive bacteria and archaea. Each subunit contains a rubredoxin-like FeS<sub>4</sub> domain and a ferritin-like four helix bundle domain surrounding the di-iron-oxo site (Fig. 19a) [63, 64]. Rbr is one component of a novel oxidative stress protection system in these microorganisms, functioning as a hydrogen peroxide reductase (peroxidase). High resolution crystallographic structures of the best characterized DvRbrs, rubrerythrin, from *Desulfovibrio vulgaris* DvRbr and its homologue nigerythrin (DvNgr) have been determined [65, 66]. Both show a 2 Å movement of one iron atom of the di-iron site from a carboxylate to a histidine ligand upon conversion of the mixed-valent ([Fe2(II),Fe1(III)]) to the diferrous state (Fig. 19b). This Glu $\leftrightarrow$ His ligand “toggling” of one iron appears to be a characteristic feature of Rbr-type di-iron sites.

## 11. Conclusions

Ferritins are members of a much larger superfamily of proteins, which are characterised by a structural motif consisting of a bundle of four parallel and anti-parallel  $\alpha$  helices. The ferritin superfamily itself is widely distributed across all three living kingdoms, in both aerobic and anaerobic organisms. Many of them, like the ribonucleotide reductase-like family of proteins (also part of the ferritin superfamily) are characterised by a carboxylate-bridged di-iron centre localised within the four-helix bundle, which seems to be a preferred biological scaffold for dioxygen binding and activation. The ferritins all form stable 24 subunit oligomeric protein shells within which a non-toxic yet biologically available iron core can be deposited, whereas the bacterial DPS proteins form dodecamers with a much smaller internal cavity.

The tertiary structures of mammalian H and L chain ferritins, bacterial FTNs and the haem-containing BFRs and the DPS proteins are very similar with extensive interactions between the central bundle of helices. However the ferritins differ from the DPS proteins by the localisation within the subunit of a fifth additional short helix. In the ferritins, this helix is at the C-terminus, and forms the channels which line the crystallographic 4-fold axes of the oligomer. In contrast, in DPS proteins, the fifth helix is located between the B and C helices of the central bundle and helps to define the 2-fold axis of the oligomer. A recent helix swapping study of BFR and DPS [67] indicates that the BC helix is less important than the E-helix for overall assembly of the oligomer, suggesting that dimer formation may play a less important role in the self assembly of the protein shell than previously thought.

The characteristic carboxylate-bridged di-iron ferroxidase sites of the ferritins, situated within the subunit itself are very similar. However, in the DPS proteins, the di-iron ferroxidase site is located at the dimer intersubunit interface. Potential entry sites for iron have also been deduced from X-ray crystallographic studies, as has the nucleation site characteristic of L chain ferritins.

## References

- [1] R.R. Crichton, Inorganic Biochemistry of Iron Metabolism from Molecular Mechanisms to Clinical Consequences, 3rd Ed., John Wiley and Sons, Chichester, 2009, pp. 183–222.
- [2] S.C. Andrews, The ferritin superfamily: structure, function and evolution of the biological iron storeman, *Biochim. Biophys. Acta* (2009).
- [3] P. Nordlund, H. Eklund, Di-iron-carboxylate proteins, *Curr. Opin. Struct. Biol.* 5 (1995) 758–766.
- [4] M.H. Szazinsky, S.J. Lippard, Correlating structure with function in bacterial multicomponent monooxygenases and related di-iron proteins, *Acc. Chem. Res.* 39 (2006) 558–566.
- [5] J.W. Drysdale, Ferritin phenotypes: structure and metabolism, *CIBS Fdn. Symp.* 51 (1977) 41–57.

- [6] F. Bou-Abdallah, The iron redox and hydrolysis chemistry of the ferritins, *Biochim. Biophys. Acta* (2009).
- [7] J.-F. Briat, F. Gaymard, Ferritins and iron storage in plants, *Biochim. Biophys. Acta* (2009).
- [8] P.D. Hempstead, S.J. Yewdall, A.R. Ferrie, et al., Comparison of the three-dimensional structures of recombinant human H and horse L ferritins at high resolution, *J. Mol. Biol.* 268 (1997) 424–448.
- [9] A. van Eerde, S. Wolterink-van Loo, J. van der Ost, B.W. Dijkstra, Fortuitous structure determination of 'as-isolated' *Escherichia coli* bacterioferritin in a novel crystal form, *Acta Cryst. F* 62 (2006) 1061–1066.
- [10] S. Macedo, C.V. Romao, E. Mitchell, et al., The nature of the di-iron site in the bacterioferritin from *Desulfovibrio desulfuricans*, *Nat. Struct. Biol.* 10 (2003) 285–290.
- [11] C.V. Romao, E.P. Mitchell, S. McSweeney, The crystal structure of *Deinococcus radiodurans* Dps protein (DR2263) reveals the presence of a novel metal centre, *J. Biol. Inorg. Chem.* 11 (2006) 891–902.
- [12] R. Fan, A.L. Boyle, V.V. Cheong, S.L. Ng, B.P. Orner, A helix swapping study of two protein cages, *Biochemistry* 48 (2009) 5623–5630.
- [13] B. Gallois, B. Langlois d'Estaintot, A.M. Michaux, et al., X-ray structure of recombinant horse L-chain apoferritin at 2.0 Å resolution: implications for stability and function, *J. Biol. Inorg. Chem.* 2 (1997) 360–367.
- [14] S. Stefanini, P. Vecchini, E. Chiancone, On the mechanism of horse spleen apoferritin assembly. A Sedimentation Velocity and Circular Dichroism Study, *Biochemistry* 26 (1987) 1831–1837.
- [15] M. Gerl, R. Jaenicke, Mechanism of the self-assembly of apoferritin from horse spleen. Cross-linking and spectroscopic analysis, *Eur. Biophys. J.* 15 (1987) 103–109.
- [16] E. Johnson, D. Cascio, M.R. Saway, M. Gingery, I. Schröder, Crystal structures of a tetrahedral open pore ferritin from the hyperthermophilic archaeon *Archaeoglobus fulgidus*, *Structure* 13 (2005) 637–648.
- [17] A.E. Hamburger, A.P. West Jr., Z.A. Hamburger, P. Hamburger, P.J. Bjorkman, Crystal structure of a secreted insect ferritin reveals a symmetrical arrangement of heavy and light chains, *J. Mol. Biol.* 349 (2005) 558–569.
- [18] T.J. Stillman, P.D. Hempstead, P.J. Artymuik, et al., The high-resolution X-ray crystallographic structure of the ferritin (EcFtnA) of *Escherichia coli*; comparison with human H ferritin (HuHF) and the structures of the Fe(3+) and Zn(2+) derivative, *J. Mol. Biol.* 307 (2001) 587–603.
- [19] M.A. Carrondo, Ferritins, iron uptake and storage from the bacterioferritin viewpoint, *EMBO J.* 22 (2003) 1959–1968.
- [20] F. Frolow, A.J. Kalb, J. Yarov, Structure of a unique twofold symmetric haem-binding site, *Nat. Struct. Biol.* 1 (1994) 453–460.
- [21] M.A. Michaux, A. Dautant, B. Gallois, et al., Structural investigation of the complexation properties between horse spleen apoferritin and metalloporphyrins, *Proteins: Struct. Funct. Genet.* 24 (1996) 314–321.
- [22] J.P. Gallivan, D.A. Dougherty, Cation- $\pi$  interactions in structural biology, *Proc. Natl. Acad. Sci. U. S. A.* 96 (1999) 9459–9464.
- [23] J. Tatur, W.R. Hagen, P.M. Mathias, Crystal structure of the ferritin from the hyperthermophilic archaeal anaerobe *Pyrococcus furiosus*, *J. Biol. Inorg. Chem.* 12 (2007) 615–630.
- [24] E.I. Steifel, G.D. Watt, Azotobacter cytochrome b557.5 is a bacterioferritin, *Nature* 279 (1979) 81–83.
- [25] G.R. Moore, F.D.A. Kadir, F.K. al-Massad, et al., Structural heterogeneity of *Pseudomonas aeruginosa* bacterioferritin, *Biochem. J.* 304 (1994) 493–497.
- [26] C.D. Miller, Y.C. Kim, M.K. Walsh, A.J. Anderson, Characterization and expression of the *Pseudomonas putida* bacterioferritin alpha subunit gene, *Gene* 247 (2000) 199–207.
- [27] N. Keren, R. Aurora, R.H.B. Pakrasi, Critical roles of bacterioferritins in iron storage and proliferation of cyanobacteria, *Plant Physiol.* 135 (2004) 1666–1673.
- [28] S. Macedo, C.V. Romao, E. Mitchell, et al., The nature of the di-iron site in the bacterioferritin from *Desulfovibrio desulfuricans*, *Nat. Struct. Biol.* 10 (2003) 285–290.
- [29] R. Watt, The movement of iron and other ions through the protein shell of ferritin, *Biochim. Biophys. Acta* (2009).
- [30] S. Stefanini, A. Desideri, P. Vecchini, T. Drakenberg, E. Chiancone, Identification of the iron entry channels in apoferritin. Chemical modification and spectroscopic studies, *Biochemistry* 28 (1989) 378–382.
- [31] A. Treffry, E.R. Bauminger, D. Hechel, et al., Defining the roles of the threefold channels in iron uptake, iron oxidation and iron-core formation in ferritin: a study aided by site-directed mutagenesis, *Biochem. J.* 296 (1993) 721–728.
- [32] S. Levi, P. Santambrogio, B. Corsi, A. Cozzi, P. Arosio, Evidence that residues exposed on the three-fold channels have active roles in the mechanism of ferritin iron incorporation, *Biochem. J.* 317 (1996) 467–473.
- [33] E.C. Theil, H. Takagi, G.W. Small, et al., The ferritin iron entry and exit problem, *Inorg. Chim. Acta* 297 (2000) 242–251.
- [34] X. Yang, P. Arosio, N.D. Chasteen, Molecular diffusion into ferritin: pathways, temperature dependence, incubation time, and concentration effects, *Biophys. J.* 78 (2000) 2049–2059.
- [35] F. Bou-Abdallah, P. Arosio, P. Santambrogio, et al., Ferrous ion binding to recombinant human H-chain ferritin. An isothermal titration calorimetry study, *Biochemistry* (2002) 11184–11891.
- [36] F. Bou-Abdallah, P. Arosio, S. Levi, C. Janus-Chandler, N.D. Chasteen, Defining metal ion inhibitor interactions with recombinant human H and L-chain ferritins and site-directed variants. An isothermal titration calorimetry study, *J. Biol. Inorg. Chem.* 8 (2003) 489–497.
- [37] C.M. Barnés, E.C. Theil, K.N. Raymond, Iron uptake in ferritin is blocked by binding of  $[\text{Cr}(\text{TREN})(\text{H}_2\text{O})(\text{OH})]^{2+}$ , a slow dissociating model for  $[\text{Fe}(\text{H}_2\text{O})_6]^{2+}$ , *Proc. Natl. Acad. Sci., U. S. A.* 99 (2002) 5195–5200.
- [38] T. Douglas, D.R. Ripoll, Calculated electrostatic gradients in recombinant human H-chain ferritin, *Protein Sci.* 1 (1998) 1083–1091.
- [39] T. Takahashi, S. Kuyucak, Functional properties of threefold and fourfold channels in ferritin deduced from electrostatic calculations, *Biophys. J.* 84 (2003) 2256–2263.
- [40] Z. Wang, C. Li, M. Ellenburg, et al., Structure of human ferritin L chain, *Acta Crystallogr. D* 62 (2006) 800–806.
- [41] T. Granier, B. Langlois d'Estaintot, B. Gallois, et al., Structural description of the active sites of mouse L-chain ferritin at 1.2 Å resolution, *J. Biol. Inorg. Chem.* 8 (2003) 105–111.
- [42] L. Toussaint, L. Bertrand, L. Hue, R.R. Crichton, J.-P. Declercq, High-resolution X-ray structures of human apoferritin H-chain mutants correlated with their activity and metal-binding sites, *J. Mol. Biol.* 365 (2007) 440–452.
- [43] R. MacKinnon, Potassium channels and the atomic basis of selective ion conduction (Nobel Lecture), *Angew. Chem. Int. Ed. Engl.* 43 (2004) 4265–4277.
- [44] A. Ilari, S. Stefanini, E. Chiancone, D. Tsernoglou, The dodecameric ferritin from *Listeria innocua* contains a novel intersubunit iron-binding site, *Nat. Struct. Biol.* 7 (2000) 38–43.
- [45] B. Ren, G. Tibbelin, T. Kajino, O. Asami, R. Ladenstein, The multi-layered structure of Dps with a novel di-nuclear ferroxidase centre, *J. Mol. Biol.* 329 (2003) 467–477.
- [46] N. Le Brun, A. Crow, A.G. Mauk, G.R. Moore, Iron core mineralization in bacterial ferritins, *Biochim. Biophys. Acta* (2009).
- [47] R.R. Crichton, F. Roman, A novel mechanism for ferritin iron oxidation and deposition, *J. Mol. Catal.* 4 (1978) 75–82.
- [48] L. Swartz, M. Kuchinskas, H. Li, T.L. Poulos, W.N. Lanzilotta, Redox-dependent structural changes in the Azotobacter vinelandii bacterioferritin: new insights into the ferroxidase and iron transport mechanism, *Biochemistry* 45 (2006) 4421–4428.
- [49] V.J. Wade, S. Levi, P. Arosio, A. Treffry, P.M. Harrison, S. Mann, Influence of site-directed modifications on the formation of iron cores in ferritin, *J. Mol. Biol.* 221 (1991) 1443–1452.
- [50] S. Levi, S.J. Yewdall, P.M. Harrison, et al., Evidence of H- and L-chains have co-operative roles in the iron-uptake mechanism of human ferritin, *Biochem. J.* 288 (1992) 591–596.
- [51] P. Santambrogio, S. Levi, A. Cozzi, B. Corsi, P. Arosio, Evidence that the specificity of iron incorporation into homopolymers of human ferritin L- and H-chains is conferred by the nucleation and ferroxidase centres, *Biochem. J.* 314 (1996) 139–144.
- [52] R.R. Crichton, A. Herbas, O. Chavez Alba, F. Roland, *J. Biol. Inorg. Chem.* 1 (1996) 567–574.
- [53] T. Granier, G. Comberton, B. Gallois, et al., Evidence of new cadmium binding sites in recombinant L-chain ferritin by anomalous Fourier map calculation Proteins, *Struct. Funct. Genet.* 31 (1998) 477–485.
- [54] T. Granier, B. Langlois d'Estaintot, B. Gallois, et al., Structural description of the active sites of mouse L-chain ferritin at 1.2 Å resolution, *J. Biol. Inorg. Chem.* 8 (2003) 105–111.
- [55] P. Santambrogio, A. Cozzi, S. Levi, et al., Functional and immunological analysis of recombinant mouse H- and L-ferritins from *Escherichia coli*, *Protein Expr. Purif.* 19 (2000) 212–218.
- [56] O. Gakh, D.Y. Smith IV, G. Isaya, Assembly of the iron-binding protein frataxin in *Saccharomyces cerevisiae* responds to dynamic changes in mitochondrial iron influx and stress level, *J. Biol. Chem.* 283 (2008) 31500–31510.
- [57] M. Bozzi, G. Mignogna, S. Stefanini, et al., A novel non-heme iron-binding ferritin related to the DNA-binding proteins of the Dps family in *Listeria innocua*, *J. Biol. Chem.* 272 (1997) 3259–3265.
- [58] A. Ilari, S. Stefanini, E. Chiancone, D. Tsernoglou, The dodecameric ferritin from *Listeria innocua* contains a novel intersubunit iron-binding site, *Nat. Struct. Biol.* 7 (2000) 38–43.
- [59] M. Su, S. Cavallo, S. Stefanini, E. Chiancone, N.D. Chasteen, The so-called *Listeria innocua* ferritin is a Dps protein. Iron incorporation, detoxification, and DNA protection properties, *Biochemistry* 44 (2005) 5572–5578.
- [60] A. Ilari, P. Ceci, D. Ferrari, et al., Iron incorporation into *Escherichia coli* Dps gives rise to a ferritin-like microcrystalline core, *J. Biol. Chem.*, 277, 37619–37623.
- [61] R.A. Grant, D.J. Filman, S.E. Finkel, R. Kolter, J.M. Hogle, The crystal structure of Dps, a ferritin homolog that binds and protects DNA, *Nature Struct. Biol.* 5 (1998) 294–303.
- [62] B. Ren, G. Tibbelin, T. Kajino, O. Asami, R. Ladenstein, The multi-layered structure of Dps with a novel di-nuclear ferroxidase centre, *J. Mol. Biol.* 329 (2003) 467–477.
- [63] F. deMaré, D.M. Kurtz, P. Nordlund, The structure of *Desulfovibrio vulgaris* rubrerythrin reveals a unique combination of rubredoxin-like FeS4 and ferritin-like di-iron domains, *Nat. Struct. Biol.* 3 (1996) 539–546.
- [64] L.C. Sieker, M. Holmes, I. Le Trong, et al., The 1.9 Å crystal structure of the 'as isolated' rubrerythrin from *Desulfovibrio vulgaris*: some surprising results, *J. Biol. Inorg. Chem.* 5 (2000) 505–513.
- [65] S. Jin, D.M. Kurtz Jr., Z.J. Liu, J. Rose, B.C. Wang, X-ray crystal structure of *Desulfovibrio vulgaris* rubrerythrin with zinc substituted into the  $[\text{Fe}(\text{SCys})_4]$  site and alternative di-iron site structures, *J. Am. Chem. Soc.* 124 (2002) 9845–9855.
- [66] R.B. Iyer, R. Silaghi-Dumitrescu, D.M. Kurtz Jr., W.N. Lanzilotta, High-resolution crystal structures of *Desulfovibrio vulgaris* (Hildenborough) rubrerythrin: facile, redox-dependent iron movement, domain interface variability, and peroxidase activity in the rubrerythrins, *J. Biol. Inorg. Chem.* 10 (2005) 407–416.
- [67] FanR, BoyleAL, CheongVV, NgSI, OrnerBP, A helix swapping study of two protein cages, *Biochemistry* 48 (2009) 5623–5630.
- [68] P.J. Kraulis, MOLSCRIPT: a program to produce both detailed and schematic plots of protein structures, *J. Appl. Crystallogr.* 24 (1991) 946–950.
- [69] E. Potterton, S. McNicolas, E. Krissinel, K. Cowtan, M. Noble, The CCP4 molecular-graphics programme, *Acta Crystallogr D* 58 (2002) 1955–1957.
- [70] A. Lewin, G.R. Moore, N.E. LeBrun, Formation of protein-coated iron minerals, *Dalton Trans.* (2005) 3597–3610.